

# Reconstruction of Baryon Fraction in Intergalactic Medium through Dispersion Measurements of Fast Radio Bursts

Ji-Ping Dai,<sup>1</sup> Jun-Qing Xia,<sup>1\*</sup>

<sup>1</sup>*Department of Astronomy, Beijing Normal University, Beijing, 100875, China*

Accepted XXX. Received YYY; in original form ZZZ

## ABSTRACT

Fast radio bursts (FRBs) probe the total column density of free electrons in the intergalactic medium (IGM) along the path of propagation through the dispersion measures (DMs) which depend on the baryon mass fraction in the IGM, i.e.,  $f_{\text{IGM}}$ . In this paper, we investigate the large-scale clustering information of DMs to study the evolution of  $f_{\text{IGM}}$ . When combining with the Planck 2018 measurements, we could give tight constraints on the evolution of  $f_{\text{IGM}}(z)$  from about  $10^4$  FRBs with the intrinsic DM scatter of  $30(1+z)$  pc/cm<sup>3</sup> spanning 80% of the sky and redshift range  $z = 0 - 3$ . Firstly, we consider the Taylor expansion of  $f_{\text{IGM}}(z)$  up to second order, and find that the mean relative standard deviation  $\sigma(f_{\text{IGM}}) \equiv \langle \sigma[f_{\text{IGM}}(z)]/f_{\text{IGM}}(z) \rangle$  is about 7.2%. In order to alleviate the dependence on fiducial model, we also adopt a non-parametric methods in this work, the local principle component analysis. We obtain the consistent, but weaker constraints on the evolution of  $f_{\text{IGM}}(z)$ , namely the mean relative standard deviation  $\sigma(f_{\text{IGM}})$  is 24.2%. With the forthcoming surveys, this could be a complimentary method to investigate the baryon mass fraction in the IGM.

**Key words:** cosmology: theory – intergalactic medium – large-scale structure of universe

## 1 INTRODUCTION

Until now, the baryon mass fraction in the intergalactic medium is still a poorly known parameter in modern cosmology. Based on the observations, Fukugita et al. (1998) presented an estimation of the global budget of baryons in all states, and they found there are about 17% of the baryons in the form of stars and their remnants. Afterwards, there are many works trying to use both numerical simulations (Cen & Ostriker 1999, 2006; Meiksin 2009) and observations (Fukugita & Peebles 2004; Shull et al. 2012; Hill et al. 2016) to study the baryon distribution. Unfortunately,  $f_{\text{IGM}}$  is still not well understood. Meiksin (2009) showed that about 90% of the baryons produced by the Big Bang are contained within the IGM at  $z \geq 1.5$ , while Shull et al. (2012) found that  $18 \pm 4\%$  of the baryons exist in the collapsed phase (galaxies, groups, clusters, circumgalactic medium) at redshift  $z \leq 0.4$ , which means  $f_{\text{IGM}} \simeq 0.82$ . These evidences show  $f_{\text{IGM}}$  could be growing with redshift, which is reasonable because there are less massive halos in the early universe (McQuinn 2014).

Recently, since the first detection of fast radio burst (Lorimer et al. 2007), it is very interesting to investigate the potential of FRBs in Cosmology (Deng & Zhang 2014;

Gao et al. 2014; Zhou et al. 2014; Fialkov & Loeb 2017; Li et al. 2018). FRBs are millisecond radio transients characterized by the excess dispersion measure with respect to the Galactic values. Since the DM of FRB is an integration of the total column density of free electrons in the IGM along the line of sight from its source, some previous works simulated the FRBs catalog with precise redshift information to constrain the evolution of baryon fraction in the IGM (Deng & Zhang 2014; Keane et al. 2016; Li et al. 2019; Wei et al. 2019).

On the other hand, there are other papers trying to use the large-scale clustering statistics of dispersion measures of FRBs to study the information of the host environment (Shirasaki et al. 2017), the reionization history (Dai & Xia 2020) and the primordial non-Gaussianity (Reischke et al. 2021). The advantage of this method is that we only need the normalized redshift distributions of FRBs catalog, instead of the precise redshift information for each FRB. In this paper, we study the auto-correlation of the fluctuations of DM from mock FRB samples span  $z = 0$  to  $z = 3$ . Together with the Planck 2018 temperature and polarization measurements, we study the constraints on the evolution of the baryon mass fraction in the IGM using both the parametric and the non-parametric methods. The rest of the paper is organized as follows. In Sec. 2 we introduce the clustering properties of the observed DM and the theoretical model

\* E-mail: xiajq@bnu.edu.cn

of the auto-correlation analysis. In Sec. 3 we explicit the fitting analysis and the data used in our calculations. The constraint results using different numerical methods are shown in Sec. 4. Finally, we present conclusions and discussions in Sec. 5.

## 2 METHODOLOGY

The observed dispersion measure  $\text{DM}_{\text{obs}}$  is defined as the integral of free electrons number density along the line of sight, which consists of the contributions from the intergalactic medium,  $\text{DM}_{\text{IGM}}$ ; the FRB host galaxy,  $\text{DM}_{\text{host}}$  and the Milky Way,  $\text{DM}_{\text{MW}}$ .  $\text{DM}_{\text{IGM}}$  from a fixed source redshift  $z_s$  and angular position  $\vec{\theta}$  is given by:

$$\text{DM}_{\text{IGM}}(\vec{\theta}, z_s) = \int_0^{z_s} \frac{dz}{H(z)} \frac{n_e(\vec{\theta}, z) f_{\text{IGM}}(z)}{(1+z)^2}, \quad (1)$$

where  $n_e(\vec{\theta}, z)$  represents the number density of free electrons which can be expressed as

$$n_e(\vec{\theta}, z) = \frac{\rho_b(\vec{\theta}, z)}{m_p} \left(1 - \frac{1}{2}Y\right) \quad (\text{for } z < 3), \quad (2)$$

where  $Y \simeq 0.24$  is the mass fraction of helium,  $\rho_b(\vec{\theta}, z)$  is the baryon mass density,  $m_p$  is the proton mass, and we have assumed both hydrogen and helium are fully ionized at  $z < 3$  (Becker et al. 2011).

In order to extract information from  $\text{DM}_{\text{IGM}}$ , we also need to determine  $\text{DM}_{\text{host}}$  and  $\text{DM}_{\text{MW}}$ . For a well-localized FRB,  $\text{DM}_{\text{MW}}$  can be determined by Galactic pulsar observations (Taylor & Cordes 1993), but deriving  $\text{DM}_{\text{host}}$  is quite difficult due to the dependences on the type of the host galaxy, the relative orientations and the near-source plasma, which are poorly known. As a phenomenological attempt, we model  $\text{DM}_{\text{host}}$  as a function of redshift by assuming the rest-frame measurements accommodate the evolution of star formation history (Luo et al. 2018; Li et al. 2019; Wei et al. 2019), i.e.,

$$\text{DM}_{\text{host}}(z) = \text{DM}_{\text{host},0} \sqrt{\frac{\text{SFR}(z)}{\text{SFR}(0)}}, \quad (3)$$

where we use the present value  $\text{DM}_{\text{host},0} = 100 \text{ pc/cm}^3$  and  $\text{SFR}(z) = \frac{0.0156+0.118z}{1+(z/3.23)^{4.66}} M_{\odot}/\text{yr}$  adopted in Hopkins & Beacom (2006) and Wei et al. (2019) as our fiducial model.

In order to reform the 2D spherical projection, we only need the normalized number distribution of FRBs catalog  $n(z)$  which can be roughly derived from the  $\text{DM}_{\text{obs}}$  (Luo et al. 2018; Zhang 2018; Batten et al. 2020; Takahashi et al. 2021), instead of the precise redshift information of each sample. Then,  $\text{DM}_{\text{IGM}}$ ,  $\text{DM}_{\text{host}}$  and  $\text{DM}_{\text{MW}}$  for an angular position  $\vec{\theta}$  can be written as,

$$\text{DM}_{\text{IGM}}(\vec{\theta}) = \int_0^{\infty} dz W_{\text{DM,IGM}}(z) \left[1 + \delta_b(\vec{\theta}, z)\right], \quad (4)$$

$$\text{DM}_{\text{host}}(\vec{\theta}) = \int_0^{\infty} dz W_{\text{DM,host}}(z) \left[1 + \delta_s(\vec{\theta}, z)\right], \quad (5)$$

$$\text{DM}_{\text{MW}}(\vec{\theta}) = \text{DM}_{\text{MW}}(\vec{\theta}) \quad (6)$$

where  $\delta_b$  and  $\delta_s$  are the baryon density perturbation and FRB number density perturbation, respectively. Recent work (Takahashi et al. 2021) shows  $\delta_b$  agrees with  $\delta_m$  at

large scales ( $k < 1 \text{ hMpc}^{-1}$ ) but is strongly suppressed at small scales. In our analysis, we adopt the fitting baryon bias factor  $b_b(k, z) \equiv \delta_b/\delta_m$  obtained by Takahashi et al. (2021). As for FRB number density perturbation, we assume FRBs form in dark matter halos, so we can express the FRB bias  $b_{\text{FRB}}(M_{\text{FRB,h}}, z) \equiv \delta_s/\delta_m$  using the fitting formula from Tinker et al. (2010), where the halo mass is set to  $M_{\text{FRB,h}} = 10^{13} h^{-1} M_{\odot}$  as our fiducial model. The window functions of Eq. (4) and Eq. (5) are

$$W_{\text{DM,IGM}}(z) = \left(1 - \frac{1}{2}Y\right) f_{\text{IGM}}(z) \frac{\bar{\rho}_{b,0}}{m_p} \frac{(1+z)}{H(z)} \int_z^{\infty} n(z) dz \quad (7)$$

$$W_{\text{DM,host}}(z) = \frac{\text{DM}_{\text{host}}(z)}{(1+z)} n(z), \quad (8)$$

where  $\bar{\rho}_{b,0}$  is the average baryon mass density at present time, and we have converted the  $\text{DM}_{\text{host}}$  from the rest-frame observer to that of the Earth observer by a factor of  $1/(1+z)$  (Ioka 2003).

Finally, the auto-correlation power spectrum of the fluctuations of  $\text{DM}_{\text{obs}}$ :  $\delta\text{DM}_{\text{obs}}(\vec{\theta}) \equiv \text{DM}_{\text{obs}}(\vec{\theta}) - \overline{\text{DM}_{\text{obs}}}$  is given by

$$C_{\ell}^{\text{DM}} = C_{\ell}^{\text{IGM,IGM}} + C_{\ell}^{\text{host,host}} + C_{\ell}^{\text{MW,MW}} + C_{\ell}^{\text{IGM,host}} + C_{\ell}^{\text{IGM,MW}} + C_{\ell}^{\text{host,MW}}. \quad (9)$$

Usually, we do not consider the contributions from  $\delta\text{DM}_{\text{MW}}(\vec{\theta})$  and its correlations with  $\delta\text{DM}_{\text{IGM}}(\vec{\theta})$  and  $\delta\text{DM}_{\text{host}}(\vec{\theta})$ . Therefore, we have three terms left:  $C_{\ell}^{\text{IGM,IGM}}$ ,  $C_{\ell}^{\text{IGM,host}}$  and  $C_{\ell}^{\text{host,host}}$ . Based on the Limber approximation (Limber 1953), we have

$$C_{\ell}^{\text{IGM,IGM}} = \int dz W_{\text{DM,IGM}}^2(z) \frac{H(z)}{\chi^2(z)} b_b^2 P_m \left(\frac{\ell+1/2}{\chi(z)}, z\right), \quad (10)$$

$$C_{\ell}^{\text{IGM,host}} = 2 \int dz W_{\text{DM,IGM}}(z) W_{\text{DM,host}}(z) \frac{H(z)}{\chi^2(z)} \times b_{\text{FRB}} b_b P_m \left(\frac{\ell+1/2}{\chi(z)}, z\right), \quad (11)$$

$$C_{\ell}^{\text{host,host}} = \int dz W_{\text{DM,host}}^2(z) \frac{H(z)}{\chi^2(z)} b_{\text{FRB}}^2 P_m \left(\frac{\ell+1/2}{\chi(z)}, z\right), \quad (12)$$

where  $\chi(z)$  is the comoving distance and  $P_m$  is the matter power spectrum.

## 3 DATA AND LIKELIHOOD

In our analysis, we includes the measurements of CMB temperature and polarization anisotropy from the Planck 2018 legacy data release (Aghanim et al. 2020), which are used to constrain the  $\Lambda\text{CDM}$  parameters. We use the combination of the `Planck` likelihood using  $TT$ ,  $TE$  and  $EE$  spectra at  $\ell \geq 30$ , the low- $\ell$  ( $\ell = 2 \sim 29$ ) temperature `Commander` likelihood and the `SimAll`  $EE$  likelihood, which is labeled as  $TT, TE, EE + \text{lowE}$  in Aghanim et al. (2020).

Then, we discuss the mock angular power spectrum used in this paper. We do not need the precise redshift information of each FRB which is hard to obtain. Instead, we can use the observed DMs to estimate the redshift distribution  $n(z)$ . Here, we assume the redshift distribution of FRBs in the redshift range  $0 < z < 3$  is  $n(z) \propto z^k e^{-z/\lambda}$  (Zhou et al. 2014), and we set  $k = 1$  and  $\lambda = 1$  as our fiducial model.

We also need to consider the noise spectrum for the observed  $\delta\text{DM}_{\text{obs}}(\vec{\theta})$ , which can be decomposed as

$$N_{\ell}^{\text{DM}} = \sqrt{\frac{2}{(2\ell+1)f_{\text{sky}}}} \left[ C_{\ell}^{\text{DM}} + N_{\ell}^{\text{host}} \right], \quad (13)$$

where  $N_{\ell}^{\text{host}}$  is the noise induced by the intrinsic scatter of DM around host galaxies (Shirasaki et al. 2017; Reischke et al. 2021; Takahashi et al. 2021):  $N_{\ell}^{\text{host}} = 4\pi f_{\text{sky}} \sigma_{\text{host}}^2 / \mathcal{N}$ . We set the intrinsic scatter of DM around host galaxies  $\sigma_{\text{host}} = 30 \text{ pc/cm}^3$  (redshift independent, i.e.,  $30(1+z) \text{ pc/cm}^3$  in the rest-frame), the sky fraction  $f_{\text{sky}} = 0.8$  and we use  $\mathcal{N} = 10^4$  FRBs span  $z = 0$  to  $z = 3$ . The mock DM angular power spectrum at  $\ell$  can be easily obtained by Gaussian sampling with the mean value  $\mu = C_{\ell}^{\text{DM}}$  and the standard deviation  $\sigma = N_{\ell}^{\text{DM}}$ .

Finally we can obtain the  $\chi^2$  function, where we have assumed the different scales are independent with each other,

$$\chi^2 = \left( \hat{C}_{\ell}^{\text{DM}} - C_{\ell}^{\text{DM}} \right) \Gamma_{\ell, \ell'}^{-1} \left( \hat{C}_{\ell'}^{\text{DM}} - C_{\ell'}^{\text{DM}} \right)^{\text{T}}, \quad (14)$$

where  $C_{\ell}^{\text{DM}}$  refer to the theoretical model and  $\hat{C}_{\ell}^{\text{DM}}$  is our mock spectrum.  $\Gamma_{\ell, \ell'} = \delta_{\ell, \ell'} (N_{\ell}^{\text{DM}})^2$  is the diagonal covariance matrix. In our analysis, we set  $\ell_{\text{max}} = 500$  due to the resolution limitation of the observed FRBs.

With these data likelihoods, we perform a global fitting analysis using the COSMOMC package (Lewis & Bridle 2002), a Markov Chain Monte Carlo (MCMC) code with a purely adiabatic initial conditions and a  $\Lambda\text{CDM}$  universe. The parameterization used in our analysis is thus:  $P \equiv \{\Omega_{\text{b}} h^2, \Omega_{\text{c}} h^2, \Theta_{\text{s}}, n_{\text{s}}, A_{\text{s}}, P_{\text{IGM}}, M_{\text{FRB, h}}, \text{DM}_{\text{host, 0}}, \Delta z\}$ , where  $\Omega_{\text{b}} h^2$  and  $\Omega_{\text{c}} h^2$  are the baryon and cold dark matter physical density,  $\Theta_{\text{s}}$  is the angular size of the sound horizon at decoupling,  $n_{\text{s}}$  and  $A_{\text{s}}$  are the spectral index and the primordial power spectrum, and  $P_{\text{IGM}}$  are the parameters which describe the evolution of  $f_{\text{IGM}}(z)$ . We also include three additional nuisance parameters  $\{M_{\text{FRB, h}}, \text{DM}_{\text{host, 0}}, \Delta z\}$  to make a more robust conclusion.  $M_{\text{FRB, h}}$  is used to account for the FRB bias uncertainty. We set this parameter vary between  $[10^{12.5}, 10^{13.2}] h^{-1} M_{\odot}$ , and the spread of FRB bias  $\Delta b_{\text{FRB}}(z)/b_{\text{FRB}}(z)$  is about 30%~60%. Since  $b_{\text{FRB}}$  can be obtained by the auto-correlation of FRB density field and cross-correlation between FRB and galaxy density field (e.g. (Shirasaki et al. 2017)), this parameter space is sufficient to include the effect of  $b_{\text{FRB}}$  with future surveys. We also vary  $\text{DM}_{\text{host, 0}}$  between  $[70, 130] \text{ pc/cm}^3$  in our MCMC analysis. With more well-localized FRBs in the future, the origin and the host environment of FRB will be better known, so the parameter space can be also sufficient in this work. The last nuisance parameter  $\Delta z$  is used to describe the uncertainty of  $n(z)$ . Recent simulations (e.g. (Batten et al. 2020; Takahashi et al. 2021)) show the probability distribution of DM at a given redshift is skewed and the inferred  $z_{\text{s}}$  is higher than the analytical mean for a given DM, thus induce a bias on  $n(z)$ . In our analysis, we take this bias into account by shifting the redshift distribution from  $n(z)$  to  $n(z + \Delta z)$ , and we have checked that using  $\Delta z = 0.1$  can eliminate this bias well. We set  $\Delta z$  vary between  $[-0.1, 0.1]$  to include this effect. What is more, the redshift distribution of FRBs also can be estimated from an empirical relation in the era of Square Kilometre Array (SKA) (Hashimoto et al. 2021), which can give us a complementary check.

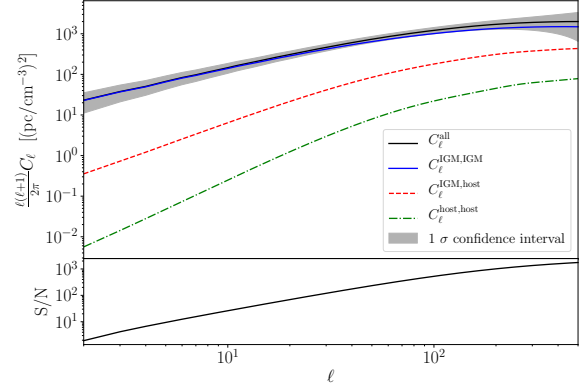


**Figure 1.** Top: The angular power spectra of DM from the auto-correlation of the IGM component (blue solid line), the cross-correlation of the IGM and the host galaxy component (red dashed line), and the auto-correlation of the host galaxy component (green dotted-dashed line). We also plot their summation (black solid line) and its  $1\sigma$  confidence interval. Bottom: Signal to noise ratio  $S/N$  as function of  $\ell_{\text{max}}$ .

## 4 CONSTRAINT RESULTS

### 4.1 Parametric method

First, we consider a parametric method by expanding  $f_{\text{IGM}}(z)$  into Taylor series up to second order (Li et al. 2019; Wei et al. 2019):

$$f_{\text{IGM}}(z) = f_{\text{IGM, 0}} + \alpha \frac{z}{1+z}, \quad (15)$$

where  $f_{\text{IGM, 0}}$  and  $\alpha$  are two free parameters. To generate the mock spectrum, we fix the fiducial values  $f_{\text{IGM, 0}} = 0.75$ ,  $\alpha = 0.25$  since  $f_{\text{IGM}}(z)$  is slowly growing with redshift, and other cosmological parameters are fixed to be the best fit values from Planck 2018 results using TT, TE, EE+lowE. In Fig. 1 we show the auto-correlation power spectra from different components and we find the contribution from the IGM component dominates the signal. We also show the  $1\sigma$  confidence interval and signal to noise ratio  $S/N \equiv \sum_{\ell=2}^{\ell_{\text{max}}} C_{\ell}^{\text{DM}} / N_{\ell}^{\text{DM}}$  as function of  $\ell_{\text{max}}$  in Fig. 1

Together with the Planck 2018 temperature and polarization measurements, our mock DM angular power spectrum could give tight constraints on the parameters:  $f_{\text{IGM, 0}} = 0.747 \pm 0.039$  and  $\alpha = 0.306 \pm 0.182$  at 68% confidence level, which are comparable with the previous works (Li et al. 2019; Wei et al. 2019). In order to present the constraints on the  $f_{\text{IGM}}$  at different redshift, we use

$$\begin{aligned} \sigma^2[f_{\text{IGM}}(z)] &\equiv \sigma^2(f_{\text{IGM, 0}}) + \sigma^2(\alpha) \left( \frac{z}{1+z} \right)^2 \\ &\quad + 2\text{COV}(f_{\text{IGM, 0}}, \alpha) \left( \frac{z}{1+z} \right) \end{aligned} \quad (16)$$

to reconstruct the redshift evolution of  $f_{\text{IGM}}(z)$  in Fig. 2, where  $\text{COV}(f_{\text{IGM, 0}}, \alpha)$  is the covariance between  $f_{\text{IGM, 0}}$  and  $\alpha$ . The orange line denotes the evolution of the fiducial model, and the grey areas are the 68% and 95% confidence intervals using this parametric method. Finally we can quantify the reconstructed uncertainty by calculating

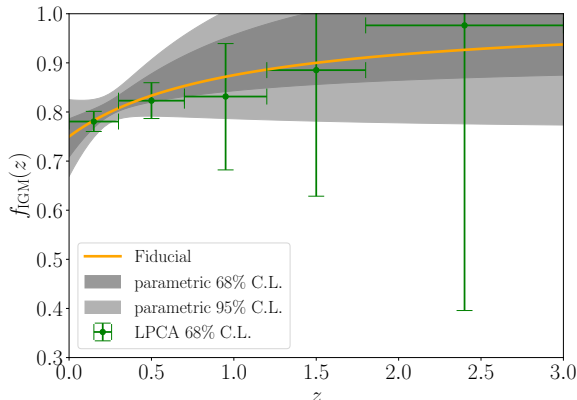


**Figure 2.** The reconstructed  $f_{\text{IGM}}(z)$  with different methods: the orange line is the fiducial model, the grey areas are the 68% and 95% confidence regions from the parametric method, the green error-bars are the 68% C.L. obtained from the LPCA method.

$\sigma(f_{\text{IGM}}) \equiv \langle \sigma[f_{\text{IGM}}(z)]/f_{\text{IGM}}(z) \rangle$  which is about 7.2%. This result with  $10^4$  FRBs is very promising, which does not need the precise redshift information of each sample.

#### 4.2 Non-parametric method

Although we already have a sufficient constraint on  $f_{\text{IGM}}(z)$ , we have to assume the evolution form first, which may lead to some biases to getting the true value. In order to conduct a parameterization-independent analysis, the simplest way is dividing the redshift range into several bins and assume  $f_{\text{IGM}}$  as a constant in each redshift bin. However, due to the strong degeneration between different bins, we can hardly obtain the proper constraints. To solve this problem, we adopt the so-called ‘‘local principle component analysis’’ (LPCA) method which has been used in the analysis of uncorrelated galaxies power spectrum (Hamilton & Tegmark 2000) and equation of state of dark energy (Huterer & Cooray 2005; Zhao et al. 2008; Zheng et al. 2014; Dai et al. 2018).

In our analysis, we divide the redshift range into 5 bins with  $0 \leq z_1 < 0.3$ ,  $0.3 \leq z_2 < 0.7$ ,  $0.7 \leq z_3 < 1.2$ ,  $1.2 \leq z_4 < 1.8$ ,  $1.8 \leq z_5 < 3$  and assume the corresponding parameter  $f_{\text{IGM}}(z_i)$  are constants. From MCMC calculation, we can compute the covariance matrix  $C$  of  $f_{\text{IGM}}(z_i)$  by marginalizing over the other parameters, and get the Fisher matrix  $F = C^{-1}$ . In order to get uncorrelated  $f_{\text{IGM}}(z_i)$ , we should rotate the original vectors into a basis where the covariance matrix is diagonal. To achieve this, we can diagonalize the Fisher matrix using an orthogonal matrix  $W$ ,  $F = W^T \Lambda W$ . Furthermore, we can define  $\hat{W}$  by absorbing the diagonal matrix  $\Lambda^{1/2}$  into  $W$ , so we have  $\hat{W}^T \hat{W} = F$ . After normalizing  $\hat{W}$ , we find the weights (rows of  $\hat{W}$ ) are almost everywhere positive and the  $i$ th element of the  $i$ th weight has the maximum value. Then the new parameters  $\hat{f}_{\text{IGM}}(z_i)$ , defined as  $\hat{f}_{\text{IGM}}(z_i) = \hat{W} f_{\text{IGM}}(z_i)$ , are uncorrelated, since they have the diagonal covariance matrix.

Using the LPCA method, we can rotate the constraints on  $f_{\text{IGM}}(z_i)$  obtained from the MCMC into the uncorrelated constraints on  $\hat{f}_{\text{IGM}}(z_i)$ , whose marginalized  $1\sigma$

constraint results are:  $\hat{f}_{\text{IGM}}(z_1) = 0.781 \pm 0.021$ ,  $\hat{f}_{\text{IGM}}(z_2) = 0.823 \pm 0.039$ ,  $\hat{f}_{\text{IGM}}(z_3) = 0.831 \pm 0.128$ ,  $\hat{f}_{\text{IGM}}(z_4) = 0.885 \pm 0.265$ ,  $\hat{f}_{\text{IGM}}(z_5) = 0.976 \pm 0.672$ , which are shown in Fig. 2 (green error bars). We find the results are consistent with the fiducial model and the constraints using the parametric method, but have larger error-bars increasing with the redshift. Based on Eq.(4) and Eq.(7), we know that, since the windows function becomes smaller as the redshift increases, the auto-correlation power spectrum is not very sensitive to  $f_{\text{IGM}}$  at higher redshifts. Consequently, the obtained constraints on  $f_{\text{IGM}}$  will also become weaker at high redshifts. The main contribution of the constraining power comes from the first three bins. We also compute the mean relative error of these five  $\hat{f}_{\text{IGM}}$  at different redshift bins, and obtain that  $\sigma(\hat{f}_{\text{IGM}}) = \langle \sigma[\hat{f}_{\text{IGM}}(z_i)]/\hat{f}_{\text{IGM}}(z_i) \rangle \simeq 24.2\%$ , which is three times larger than that using the parametric method.

## 5 CONCLUSIONS AND DISCUSSIONS

In this paper, we apply the auto-correlation power spectrum of  $\delta\text{DM}$  from the mock DM angular power spectrum to constrain the baryon mass fraction in the IGM. The main advantage of this method is that the precise redshift measurements are not necessary. We only need a rough redshift distribution from observations. Using the auto-correlation power spectrum from  $10^4$  FRBs with the host DM scatter of  $30(1+z)$  pc/cm<sup>3</sup> spanning 80% of the sky and redshift range  $z = 0 - 3$ , together with the Planck 2018 temperature and polarization measurements, we can obtain a very tight constraint on the evolution of  $f_{\text{IGM}}(z)$  if we use the simple Taylor expansion up to second order, and the reconstructed mean relative standard deviation is  $\sigma(f_{\text{IGM}}) \simeq 7.2\%$ . Furthermore, we adopt the LPCA methods to constrain the evolution of  $f_{\text{IGM}}$ . We obtain very weak constraints on  $f_{\text{IGM}}(z_i)$  at higher redshifts, which leads to a larger uncertainty  $\sigma(f_{\text{IGM}}) \simeq 24.2\%$ .

We must mention that the intrinsic scatter of DM around host galaxies  $\sigma_{\text{host}}$  is still uncertain. To demonstrate the robustness of our analysis, we also use  $\sigma_{\text{host}} = 100$  pc/cm<sup>3</sup> to constrain the parametric model (Eq.(15)). The constraints are:  $f_{\text{IGM},0} = 0.752 \pm 0.092$  and  $\alpha = 0.283 \pm 0.394$ , which are twice times larger than the results when  $\sigma_{\text{host}} = 30$  pc/cm<sup>3</sup>. Recent works (e.g. (Hashimoto et al. 2020)) show FRBs will be detected with SKA at a rate of  $\sim 10^3 - 10^4$  (sky<sup>-1</sup>day<sup>-1</sup>). Since shot noise is proportion to  $\sigma_{\text{host}}^2/N$ ,  $10^5$  FRBs with the intrinsic scatter  $\sigma_{\text{host}} = 100$  pc/cm<sup>3</sup> may have comparable results obtained in our analysis, and it is accessible with the future SKA survey.

Finally, we discuss if the expected constraints on  $f_{\text{IGM}}$  can exclude some models. The ideal case is we can directly select models with the non-parametric method. In Fig. 3 we plot five mean DM- $z$  relations. Results from Ioka (2003) and Zhang (2018) are analytical formulations. Ioka (2003) assumes the Universe is homogeneously filled with ionised hydrogen alone, and Zhang (2018) includes helium reionization and uses  $f_{\text{IGM}} = 0.85$  to exclude baryons locked inside galaxies. These two models can be seen as the upper-limit and lower-limit to the slope of the DM- $z$  relation (Batten et al. 2020). On the other hand, McQuinn (2014); Dolag et al. (2015); Batten et al. (2020) both use simulations to estimate the DM- $z$  relations. In the bottom panel of Fig. 3

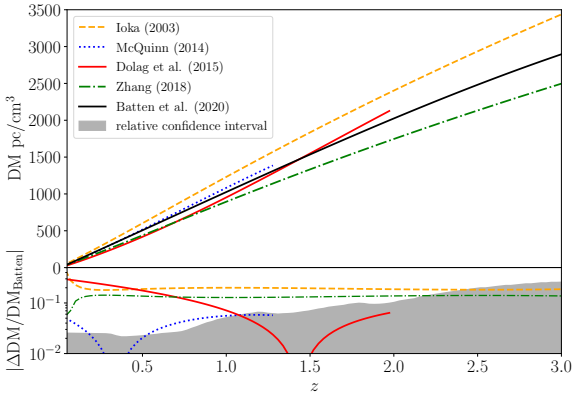


**Figure 3.** Top: The mean DM- $z$  relations from the past works. Bottom: The relative differences between Batten et al. (2020)’s result and the others results  $|\text{DM}_{\text{others}} - \text{DM}_{\text{Batten}}|/\text{DM}_{\text{Batten}}$ . To check the ability to select models, we need compare these relative differences with relative confidence interval of DM( $z$ ) obtained by LPCA method. In our analysis, we calculate DM( $z$ ) for each step in the MCMC calculation and estimate  $\sigma_{\text{DM}}(z)/\text{DM}(z)$  at each redshift. The result is also shown in the bottom panel of Fig. 3 (gray region). We can find the expected constraints on  $f_{\text{IGM}}$  in our work can be used to exclude models, especially at lower redshifts.

we plot the relative differences between Batten et al. (2020)’s result and the others results  $|\text{DM}_{\text{others}} - \text{DM}_{\text{Batten}}|/\text{DM}_{\text{Batten}}$ . To check the ability to select models, we need compare these relative differences with relative confidence interval of DM( $z$ ) obtained by LPCA method. In our analysis, we calculate DM( $z$ ) for each step in the MCMC calculation and estimate  $\sigma_{\text{DM}}(z)/\text{DM}(z)$  at each redshift. The result is also shown in the bottom panel of Fig. 3 (gray region). We can find the expected constraints on  $f_{\text{IGM}}$  in our work can be used to exclude models, especially at lower redshifts.

With the forthcoming surveys, this could be a complementary method to investigate the baryon mass fraction in the IGM and the other cosmology problems, e.g., the equation of state of dark energy, Hubble constant, etc.

## 6 DATA AVAILABILITY

The measurements of CMB temperature and polarization anisotropy from the Planck 2018 legacy data release are available in Aghanim et al. (2020) and can be downloaded from <http://pla.esac.esa.int/pla/index.html#home>. The mock DM angular power spectrum will be shared on reasonable request to the corresponding author.

## ACKNOWLEDGEMENTS

We thank Z.-X. Li and H. Gao for useful discussions. This work is supported by the National Science Foundation of China under grants No. U1931202 and 12021003, and the National Key R&D Program of China under grant No. 2017YFA0402600.

## REFERENCES

Aghanim N., et al., 2020, *Astron. Astrophys.*, 641, A6  
 Batten A. J., Duffy A. R., Wijers N., Gupta V., Flynn C., Schaye J., Ryan-Weber E., 2020, arXiv: 2011.14547

- Becker G. D., Bolton J. S., Haehnelt M. G., Sargent W. L. W., 2011, *Mon. Not. Roy. Astron. Soc.*, 410, 1096  
 Cen R., Ostriker J. P., 1999, *Astrophys. J.*, 514, 1  
 Cen R., Ostriker J. P., 2006, *Astrophys. J.*, 650, 560  
 Dai J.-P., Xia J.-Q., 2020, arXiv: 2004.11276  
 Dai J.-P., Yang Y., Xia J.-Q., 2018, *Astrophys. J.*, 857, 9  
 Deng W., Zhang B., 2014, *Astrophys. J.*, 783, L35  
 Dolag K., Gaensler B. M., Beck A. M., Beck M. C., 2015, *Mon. Not. Roy. Astron. Soc.*, 451, 4277  
 Fialkov A., Loeb A., 2017, *Astrophys. J.*, 846, L27  
 Fukugita M., Peebles P. J. E., 2004, *Astrophys. J.*, 616, 643  
 Fukugita M., Hogan C. J., Peebles P. J. E., 1998, *Astrophys. J.*, 503, 518  
 Gao H., Li Z., Zhang B., 2014, *Astrophys. J.*, 788, 189  
 Hamilton A. J. S., Tegmark M., 2000, *Mon. Not. Roy. Astron. Soc.*, 312, 285  
 Hashimoto T., et al., 2020, *Mon. Not. Roy. Astron. Soc.*, 497, 4107  
 Hashimoto T., et al., 2021, *MNRAS*, 502, 2346  
 Hill J. C., Ferraro S., Battaglia N., Liu J., Spergel D. N., 2016, *Phys. Rev. Lett.*, 117, 051301  
 Hopkins A. M., Beacom J. F., 2006, *Astrophys. J.*, 651, 142  
 Huterer D., Cooray A., 2005, *Phys. Rev.*, D71, 023506  
 Ioka K., 2003, *Astrophys. J.*, 598, L79  
 Keane E. F., et al., 2016, *Nature*, 530, 453  
 Lewis A., Bridle S., 2002, *Phys. Rev.*, D66, 103511  
 Li Z.-X., Gao H., Ding X.-H., Wang G.-J., Zhang B., 2018, *Nature Commun.*, 9, 3833  
 Li Z., Gao H., Wei J.-J., Yang Y.-P., Zhang B., Zhu Z.-H., 2019, *Astrophys. J.*, 876, 146  
 Limber D. N., 1953, *The Astrophysical Journal*, 117, 134  
 Lorimer D. R., Bailes M., McLaughlin M. A., Narkevic D. J., Crawford F., 2007, *Science*, 318, 777  
 Luo R., Lee K., Lorimer D. R., Zhang B., 2018, *Mon. Not. Roy. Astron. Soc.*, 481, 2320  
 McQuinn M., 2014, *Astrophys. J.*, 780, L33  
 Meiksin A. A., 2009, *Rev. Mod. Phys.*, 81, 1405  
 Reischke R., Hagstotz S., Lilow R., 2021, *Phys. Rev. D*, 103, 023517  
 Shirasaki M., Kashiyama K., Yoshida N., 2017, *Phys. Rev.*, D95, 083012  
 Shull J. M., Smith B. D., Danforth C. W., 2012, *Astrophys. J.*, 759, 23  
 Takahashi R., Ioka K., Mori A., Funahashi K., 2021, *MNRAS*, 502, 2615  
 Taylor J. H., Cordes J. M., 1993, *Astrophys. J.*, 411, 674  
 Tinker J. L., Robertson B. E., Kravtsov A. V., Klypin A., Warren M. S., Yepes G., Gottlober S., 2010, *Astrophys. J.*, 724, 878  
 Wei J.-J., Li Z., Gao H., Wu X.-F., 2019, *JCAP*, 1909, 039  
 Zhang B., 2018, *Astrophys. J.*, 867, L21  
 Zhao G.-B., Huterer D., Zhang X., 2008, *Phys. Rev.*, D77, 121302  
 Zheng W., Li S.-Y., Li H., Xia J.-Q., Li M., Lu T., 2014, *JCAP*, 1408, 030  
 Zhou B., Li X., Wang T., Fan Y.-Z., Wei D.-M., 2014, *Phys. Rev.*, D89, 107303

This paper has been typeset from a  $\text{\TeX}/\text{\LaTeX}$  file prepared by the author.